Hindawi Publishing Corporation
Advances in Mechanical Engineering
Volume 2014, Article ID 813510, 10 pages
http://dx.doi.org/10.1155/2014/813510

Research Article

Performance Analyses of IDEAL Algorithm on Highly Skewed Grid System

Dongliang Sun,[1,2] Jinliang Xu,[1,2] and Peng Ding[3]

[1] *Beijing Key Laboratory of Multiphase Flow and Heat Transfer, North China Electric Power University, Beijing 102206, China*
[2] *Beijing Key Laboratory of Energy Safety and Clean Utilization, North China Electric Power University, Beijing 102206, China*
[3] *College of Storage & Transportation and Architectural Engineering, China University of Petroleum (Hua Dong), Qingdao, Shandong 266555, China*

Correspondence should be addressed to Jinliang Xu; xjl@ncepu.edu.cn

Received 23 January 2014; Accepted 10 February 2014; Published 16 March 2014

Academic Editor: Bo Yu

IDEAL is an efficient segregated algorithm for the fluid flow and heat transfer problems. This algorithm has now been extended to the 3D nonorthogonal curvilinear coordinates. Highly skewed grids in the nonorthogonal curvilinear coordinates can decrease the convergence rate and deteriorate the calculating stability. In this study, the feasibility of the IDEAL algorithm on highly skewed grid system is analyzed by investigating the lid-driven flow in the inclined cavity. It can be concluded that the IDEAL algorithm is more robust and more efficient than the traditional SIMPLER algorithm, especially for the highly skewed and fine grid system. For example, at $\theta = 5^{\circ}$ and grid number $= 70 \times 70 \times 70$, the convergence rate of the IDEAL algorithm is 6.3 times faster than that of the SIMPLER algorithm, and the IDEAL algorithm can converge almost at any time step multiple.

1. Introduction

SIMPLE [1] is the first pressure-correction algorithm, which was proposed by Patankar and Spalding in 1972. This algorithm is still widely used until now and is one of the most important solvers in FLUENT software. However, there are two major approximations in the SIMPLE algorithm. The first is that the initial pressure and velocity fields are assumed independently, thus neglecting the coupling between pressure and velocity. The second is that the velocity corrections of the neighboring grids are neglected in order to make the final pressure-correction equation manageable. These two approximations do not affect the final converged solutions but influence the convergence rate and robustness of the algorithm greatly [2]. For overcoming one or both of the approximations mentioned above, a series of algorithms have been proposed since the birth of the SIMPLE algorithm, such as SIMPLER (1981) [3], SIMPLEST (1981) [4, 5], SIMPLEC (1984) [6], PISO (1985) [7, 8], SIMPLEX (1985) [9, 10], FIMOSE (1985) [11], CTS SIMPLE (1986) [12], SIMPLESSE (1993) [13], SIMPLESSEC (1997) [14], SIMPLET (1998) [15], SOAR (2000) [16], MSIMPLER (2001) [17], and CSIMPLER (2005) [18]. The common characteristic of the above-mentioned algorithms is that a pressure-correction term is introduced to improve the velocity and pressure, leading to the neglect of the velocity corrections of the neighboring grids. Hence the second approximation is not overcome and these algorithms are only semi-implicit.

In 2004, Tao et al. [19, 20] proposed a novel CLEAR algorithm. Different from other algorithms, the algorithm improves the velocity and pressure by solving a pressure equation directly, avoiding the introduction of a pressure-correction term and a velocity-correction term. Thus the second approximation of the SIMPLE algorithm is overcome, making the algorithm fully implicit. However, the robustness of the CLEAR algorithm is somewhat weakened by directly solving the pressure equation. Therefore, further improvement should be made to develop a more efficient and robust algorithm.

To overcome the disadvantage of the CLEAR algorithm, the present authors proposed an IDEAL algorithm [21, 22] in 2008. In the IDEAL algorithm, there exist two inner iteration

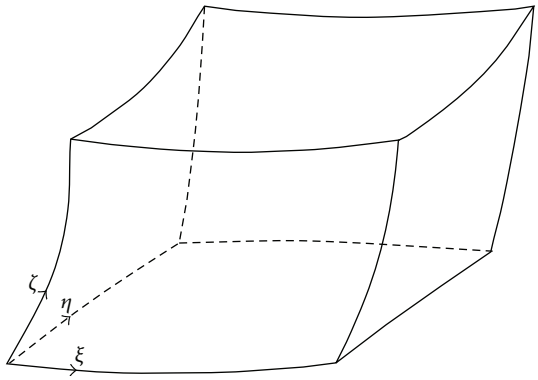

Figure 1: 3D nonorthogonal curvilinear coordinate system.

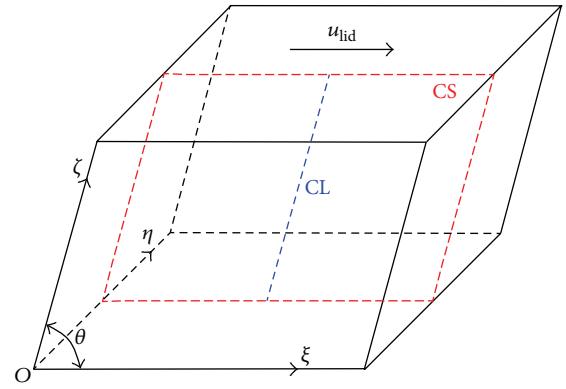

Figure 2: Schematic diagram of the 3D inclined cavity.

processes for pressure field solution at each iteration level. The first inner iteration process for pressure equation can almost completely overcome the first approximation of the SIMPLE algorithm. The second inner iteration process can almost completely overcome the second approximation of the SIMPLE algorithm. Thus the coupling between velocity and pressure is fully guaranteed, greatly enhancing the convergence rate and stability of the solution process. The IDEAL algorithm has now been extended to the orthogonal coordinates [23–25] and the nonorthogonal curvilinear coordinates [26].

The quality of the grid plays a significant role in the convergence rate and stability of the solution process. Highly skewed grids in the nonorthogonal curvilinear coordinates can decrease the convergence rate and deteriorate the calculating stability. The skewness is defined as the difference between the shape of the grid and the shape of an equivalent orthogonal grid. For example, optimal grids, that is, nonskewed grids, will have vertex angles close to 90 degrees. In this study, the feasibility of the IDEAL algorithm for the flow on highly skewed grids is investigated. The typical flow problem is the lid-driven flow, which has served over and over again in CFD/NHT as a classical problem for testing the developed algorithms. Despite its simple geometry, the lid-driven flow retains a rich fluid flow structure manifested by multiple counter-rotating recirculating regions on the corners. Due to the flow complexity and convergence difficulty, the lid-driven flow in the inclined cavity is adopted to analyze the solving performance of the IDEAL algorithm on highly skewed grid system.

In the following presentation, the governing equations are firstly introduced in Section 2. The solution procedure of the IDEAL algorithm in the 3D nonorthogonal curvilinear coordinates is briefly reviewed in Section 3. The effect of the grid skewness on the solving performance of the IDEAL algorithm is analyzed in Section 4. The conclusions are summarized in the end of the paper.

2. Governing Equations

The incompressible laminar flow is considered in this study. Figure 1 shows a 3D nonorthogonal curvilinear coordinate system (ξ, η, ζ). The corresponding governing equations in this coordinate system are written as the follows.

Continuity equation:

$$\frac{\partial}{\partial \xi}(\rho U) + \frac{\partial}{\partial \eta}(\rho V) + \frac{\partial}{\partial \zeta}(\rho W) = 0. \tag{1}$$

Momentum equations:

$$\begin{aligned}
&\frac{\partial}{\partial \xi}(\rho U u) + \frac{\partial}{\partial \eta}(\rho V u) + \frac{\partial}{\partial \zeta}(\rho W u) \\
&\quad = \frac{\partial}{\partial \xi}\left(\frac{\chi}{J}\eta\frac{\partial u}{\partial \xi}\right) + \frac{\partial}{\partial \eta}\left(\frac{\beta}{J}\eta\frac{\partial u}{\partial \eta}\right) + \frac{\partial}{\partial \zeta}\left(\frac{\gamma}{J}\eta\frac{\partial u}{\partial \zeta}\right) \\
&\qquad - \chi_1\frac{\partial p}{\partial \xi} - \beta_1\frac{\partial p}{\partial \eta} - \gamma_1\frac{\partial p}{\partial \zeta} + JS'_u, \\
&\frac{\partial}{\partial \xi}(\rho U v) + \frac{\partial}{\partial \eta}(\rho V v) + \frac{\partial}{\partial \zeta}(\rho W v) \\
&\quad = \frac{\partial}{\partial \xi}\left(\frac{\chi}{J}\eta\frac{\partial v}{\partial \xi}\right) + \frac{\partial}{\partial \eta}\left(\frac{\beta}{J}\eta\frac{\partial v}{\partial \eta}\right) + \frac{\partial}{\partial \zeta}\left(\frac{\gamma}{J}\eta\frac{\partial v}{\partial \zeta}\right) \\
&\qquad - \chi_2\frac{\partial p}{\partial \xi} - \beta_2\frac{\partial p}{\partial \eta} - \gamma_2\frac{\partial p}{\partial \zeta} + JS'_v, \\
&\frac{\partial}{\partial \xi}(\rho U w) + \frac{\partial}{\partial \eta}(\rho V w) + \frac{\partial}{\partial \zeta}(\rho W w) \\
&\quad = \frac{\partial}{\partial \xi}\left(\frac{\chi}{J}\eta\frac{\partial w}{\partial \xi}\right) + \frac{\partial}{\partial \eta}\left(\frac{\beta}{J}\eta\frac{\partial w}{\partial \eta}\right) + \frac{\partial}{\partial \zeta}\left(\frac{\gamma}{J}\eta\frac{\partial w}{\partial \zeta}\right) \\
&\qquad - \chi_3\frac{\partial p}{\partial \xi} - \beta_3\frac{\partial p}{\partial \eta} - \gamma_3\frac{\partial p}{\partial \zeta} + JS'_w.
\end{aligned} \tag{2}$$

In (1)-(2), U, V, and W are contravariant velocities and can be expressed as

$$\begin{aligned}
U &= \chi_1 u + \chi_2 v + \chi_3 w, \\
V &= \beta_1 u + \beta_2 v + \beta_3 w, \\
W &= \gamma_1 u + \gamma_2 v + \gamma_3 w.
\end{aligned} \tag{3}$$

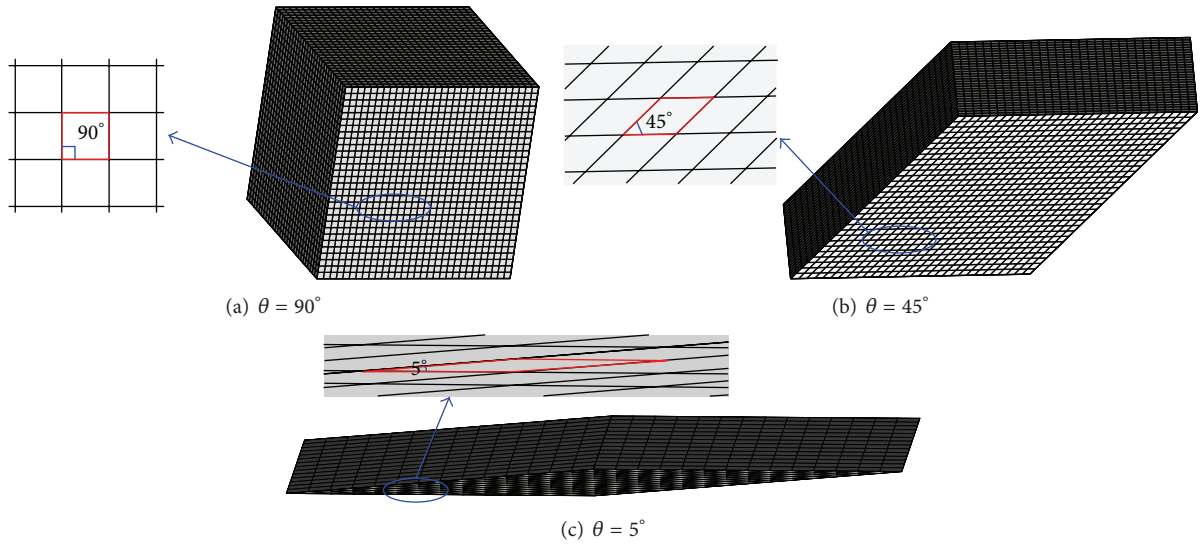

(a) $\theta = 90^\circ$ (b) $\theta = 45^\circ$

(c) $\theta = 5^\circ$

FIGURE 3: Body-fitted grid systems for the 3D inclined cavity.

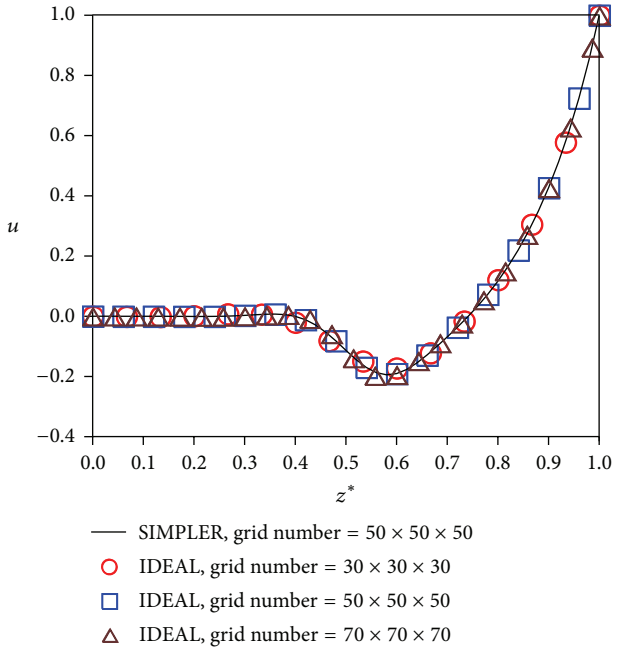

FIGURE 4: Comparison of u velocity profiles along the central line "CL" at $\theta = 5^\circ$ and Re = 500.

The governing equations (1)-(2) are discretized on the body-fitted collocated grid system with the finite volume method (FVM) [27].

Discretized continuity equation:

$$(\rho U)_e \Delta\eta\Delta\zeta - (\rho U)_w \Delta\eta\Delta\zeta + (\rho V)_n \Delta\xi\Delta\zeta - (\rho V)_s \Delta\xi\Delta\zeta + (\rho W)_t \Delta\xi\Delta\eta - (\rho W)_b \Delta\xi\Delta\eta = 0. \quad (4)$$

Discretized momentum equations:

$$\frac{a_P^u}{\alpha_u} u_P = \sum_{nb} a_{nb}^u u_{nb} + b_P^u + (1-\alpha_u)\frac{a_P^u}{\alpha_u} u_P^0 - \left(\chi_1 \frac{\partial p}{\partial \xi}\right)_P \times \Delta\xi\Delta\eta\Delta\zeta - \left(\beta_1 \frac{\partial p}{\partial \eta}\right)_P \Delta\xi\Delta\eta\Delta\zeta - \left(\gamma_1 \frac{\partial p}{\partial \zeta}\right)_P \Delta\xi\Delta\eta\Delta\zeta,$$

$$\frac{a_P^v}{\alpha_v} v_P = \sum_{nb} a_{nb}^v v_{nb} + b_P^v + (1-\alpha_v)\frac{a_P^v}{\alpha_v} v_P^0 - \left(\chi_2 \frac{\partial p}{\partial \xi}\right)_P \times \Delta\xi\Delta\eta\Delta\zeta - \left(\beta_2 \frac{\partial p}{\partial \eta}\right)_P \Delta\xi\Delta\eta\Delta\zeta - \left(\gamma_2 \frac{\partial p}{\partial \zeta}\right)_P \Delta\xi\Delta\eta\Delta\zeta,$$

$$\frac{a_P^w}{\alpha_w} w_P = \sum_{nb} a_{nb}^w w_{nb} + b_P^w + (1-\alpha_w)\frac{a_P^w}{\alpha_w} w_P^0 - \left(\chi_3 \frac{\partial p}{\partial \xi}\right)_P \times \Delta\xi\Delta\eta\Delta\zeta - \left(\beta_3 \frac{\partial p}{\partial \eta}\right)_P \Delta\xi\Delta\eta\Delta\zeta - \left(\gamma_3 \frac{\partial p}{\partial \zeta}\right)_P \Delta\xi\Delta\eta\Delta\zeta, \quad (5)$$

where α_u, α_v, and α_w are the velocity underrelaxation factors. The SGSD scheme [28] is adopted for the convection terms in the momentum equations. Based on the nodal velocities, the interfacial contravariant velocities are calculated by the modified momentum interpolation method (MMIM) [29]

$$U_e = \widetilde{U}_e - B_e^U \left(\frac{\partial p}{\partial \xi}\right)_e,$$
$$V_n = \widetilde{V}_n - C_n^V \left(\frac{\partial p}{\partial \eta}\right)_n, \quad (6)$$
$$W_t = \widetilde{W}_t - D_t^W \left(\frac{\partial p}{\partial \zeta}\right)_t.$$

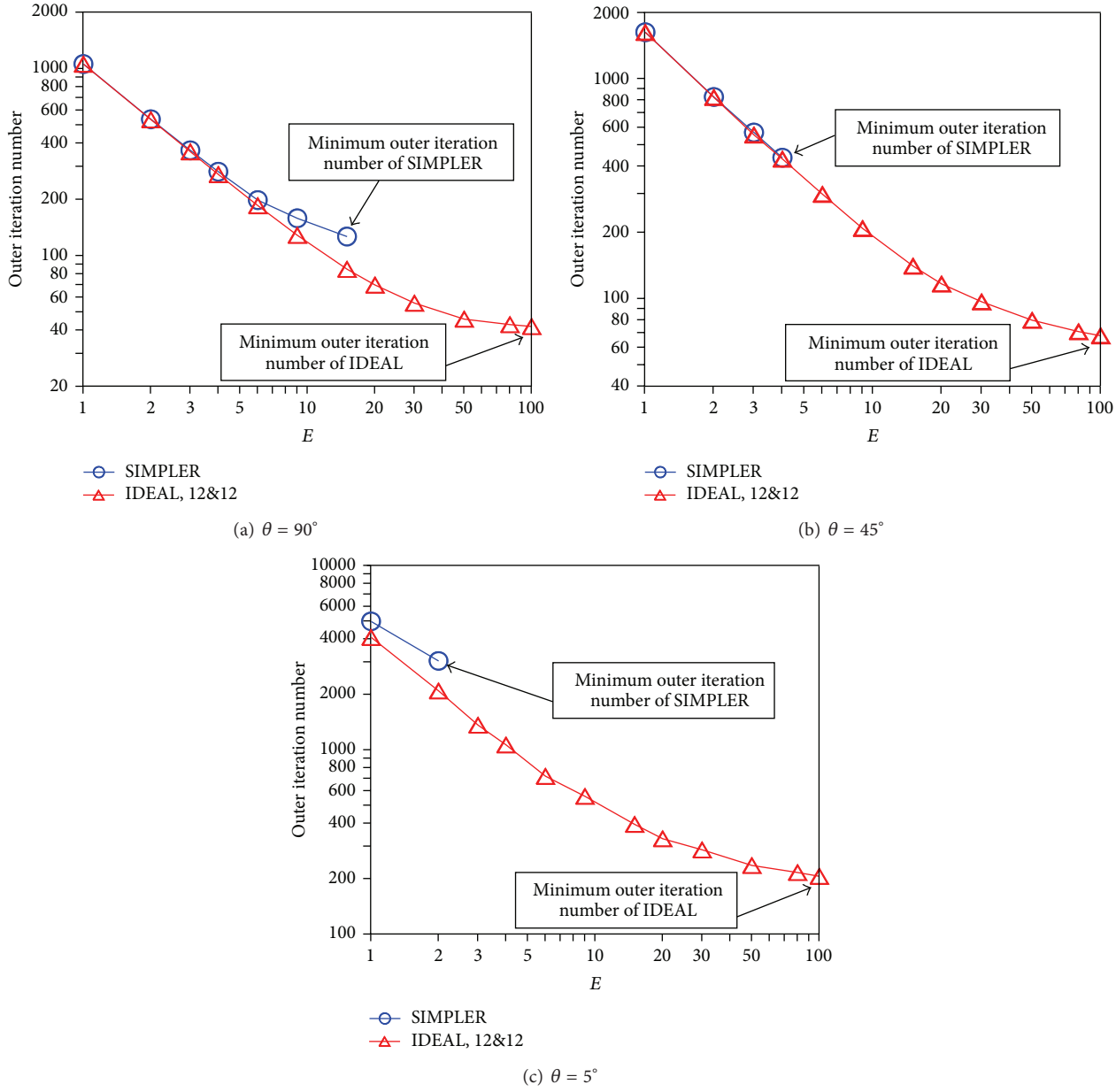

FIGURE 5: Comparison of outer iteration number between IDEAL and SIMPLER for different inclination angles (Re = 500, grid number = 50 × 50 × 50).

3. Brief Review of IDEAL in 3D Nonorthogonal Curvilinear Coordinates

Based on the body-fitted collocated grid system in the 3D nonorthogonal curvilinear coordinates, the major points of the IDEAL algorithm are reviewed in the following.

Step 1. Assume initial nodal velocities and initial interfacial contravariant velocities.

Step 2. Calculate the coefficients and source terms of the discretized momentum equations (5) by the initial velocity field.

The First Inner Iteration Process for Pressure Question

Step 3. Calculate the interfacial pseudocontravariant velocities $\widetilde{U}_e^0$, $\widetilde{V}_n^0$, and $\widetilde{W}_t^0$ by the MMIM.

Step 4. Solve the pressure by the pressure equation (7), and obtain the temporary pressure p^{Temp}

$$a_P^p p_P^{\text{Temp}} = \sum a_{nb}^p p_{nb}^{\text{Temp}} + b_P^p,$$
$$a_P^p = a_E^p + a_W^p + a_N^p + a_S^p + a_T^p + a_B^p,$$
$$a_E^p = \rho_e B_e^U \left(\frac{\Delta\eta\Delta\zeta}{\delta\xi_e}\right), \qquad a_W^p = \rho_w B_w^U \left(\frac{\Delta\eta\Delta\zeta}{\delta\xi_w}\right),$$

$$a_N^p = \rho_n C_n^V \left(\frac{\Delta\xi\Delta\zeta}{\delta\eta_n}\right), \qquad a_S^p = \rho_s C_s^V \left(\frac{\Delta\xi\Delta\zeta}{\delta\eta_s}\right),$$
$$a_T^p = \rho_t D_t^W \left(\frac{\Delta\xi\Delta\eta}{\delta\zeta_t}\right), \qquad a_B^p = \rho_b D_b^W \left(\frac{\Delta\xi\Delta\eta}{\delta\zeta_b}\right),$$
$$b_P^p = \rho_w \widetilde{U}_w^0 \Delta\eta\Delta\zeta - \rho_e \widetilde{U}_e^0 \Delta\eta\Delta\zeta + \rho_s \widetilde{V}_s^0 \Delta\xi\Delta\zeta - \rho_n \widetilde{V}_n^0 \Delta\xi\Delta\zeta + \rho_b \widetilde{W}_b^0 \Delta\xi\Delta\eta - \rho_t \widetilde{W}_t^0 \Delta\xi\Delta\eta. \tag{7}$$

Equation (7) is obtained by substituting (6) into the discretized continuity equation (4).

Step 5. Calculate the temporary nodal velocities u_P^{Temp}, v_P^{Temp}, and w_P^{Temp} from the explicit discretized momentum equations by the temporary pressure p^{Temp}. Then one inner iteration step is finished and the next inner iteration step will be started.

Step 6. Regard u_P^{Temp}, v_P^{Temp}, w_P^{Temp}, and p^{Temp} as $u_P^{P\text{Temp}}$, $v_P^{P\text{Temp}}$, $w_P^{P\text{Temp}}$, and $p^{P\text{Temp}}$. Return to Step 3, and all the superscripts "0" in Steps 3 and 4 are replaced by "PTemp." Repeat such iteration process composed of Steps 3, 4, and 5 until the iteration times are equal to the prespecified times $N1$. After the first inner iteration process is finished, the final temporary pressure p^{Temp} is regarded as the initial pressure p^*.

Step 7. Solve the discretized momentum equations (5) by the initial velocity and pressure, and obtain the intermediate nodal velocities u_P^*, v_P^*, and w_P^*.

The Second Inner Iteration Process for Pressure Question

Step 8. Calculate the interfacial pseudocontravariant velocities $\widetilde{U}_e^*$, $\widetilde{V}_n^*$, and $\widetilde{W}_t^*$ by the MMIM.

Step 9. Solve the pressure again by the pressure equation (8), and obtain the temporary pressure p^{Temp}

$$a_P^p p_P^{\text{Temp}} = \sum a_{nb}^p p_{nb}^{\text{Temp}} + b_P^p,$$
$$a_P^p = a_E^p + a_W^p + a_N^p + a_S^p + a_T^p + a_B^p,$$
$$a_E^p = \rho_e B_e^U \left(\frac{\Delta\eta\Delta\zeta}{\delta\xi_e}\right), \qquad a_W^p = \rho_w B_w^U \left(\frac{\Delta\eta\Delta\zeta}{\delta\xi_w}\right),$$
$$a_N^p = \rho_n C_n^V \left(\frac{\Delta\xi\Delta\zeta}{\delta\eta_n}\right), \qquad a_S^p = \rho_s C_s^V \left(\frac{\Delta\xi\Delta\zeta}{\delta\eta_s}\right),$$
$$a_T^p = \rho_t D_t^W \left(\frac{\Delta\xi\Delta\eta}{\delta\zeta_t}\right), \qquad a_B^p = \rho_b D_b^W \left(\frac{\Delta\xi\Delta\eta}{\delta\zeta_b}\right),$$
$$b_P^p = \rho_w \widetilde{U}_w^* \Delta\eta\Delta\zeta - \rho_e \widetilde{U}_e^* \Delta\eta\Delta\zeta + \rho_s \widetilde{V}_s^* \Delta\xi\Delta\zeta - \rho_n \widetilde{V}_n^* \Delta\xi\Delta\zeta + \rho_b \widetilde{W}_b^* \Delta\xi\Delta\eta - \rho_t \widetilde{W}_t^* \Delta\xi\Delta\eta. \tag{8}$$

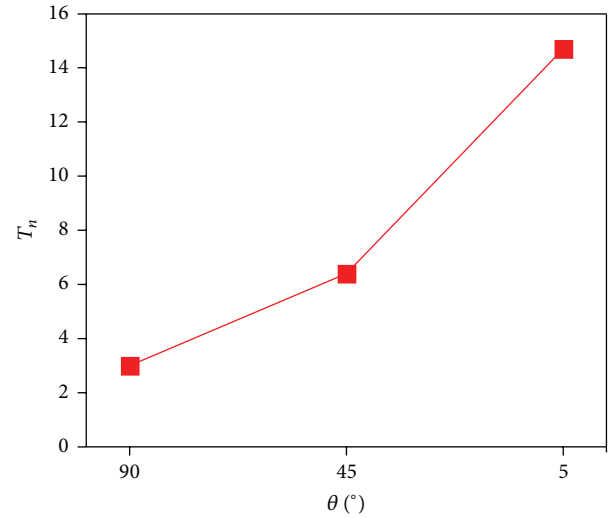

Figure 6: Times of outer iteration number of SIMPLER over that of IDEAL for different inclination angles (Re = 500, grid number = 50 × 50 × 50).

Step 10. Calculate the temporary nodal velocities u_P^{Temp}, v_P^{Temp}, and w_P^{Temp} from the explicit discretized momentum equations by the temporary pressure p^{Temp}. Then one inner iteration step is finished and the next inner iteration step will be started.

Step 11. Regard u_P^{Temp}, v_P^{Temp}, w_P^{Temp}, and p^{Temp} as $u_P^{P\text{Temp}}$, $v_P^{P\text{Temp}}$, $w_P^{P\text{Temp}}$, and $p^{P\text{Temp}}$. Return to Step 8, and all the superscripts "$*$" in Steps 8 and 9 are replaced by "PTemp." Repeat such iteration process composed of Steps 8, 9, and 10 until the iteration times are equal to the prespecified times $N2$. After the second inner iteration process is finished, the final temporary velocities are regarded as the final velocities.

Step 12. Regard the final velocities as the initial velocities of the next iteration level; then return to Step 2. Repeat such iterative procedure until convergence is reached.

In the IDEAL algorithm the first inner iteration times $N1$ and the second inner iteration times $N2$ (hereafter $N1$ & $N2$) can be adjusted to control the convergence rate and stability of the solution process. $N1$ & $N2$ is set as 12 & 12 to make the later simulation.

4. Numerical Analyses of IDEAL on Highly Skewed Grid System

4.1. Definition of Time Step Multiple. In the following, the underrelaxation factors are set to be the same for the three velocity components, that is, $\alpha_u = \alpha_v = \alpha_w = \alpha$. For the convenience of presentation, the time step multiple E is defined, which relates to the underrelaxation factor α by the following equation:

$$E = \frac{\alpha}{1-\alpha} \quad (0 < \alpha < 1). \tag{9}$$

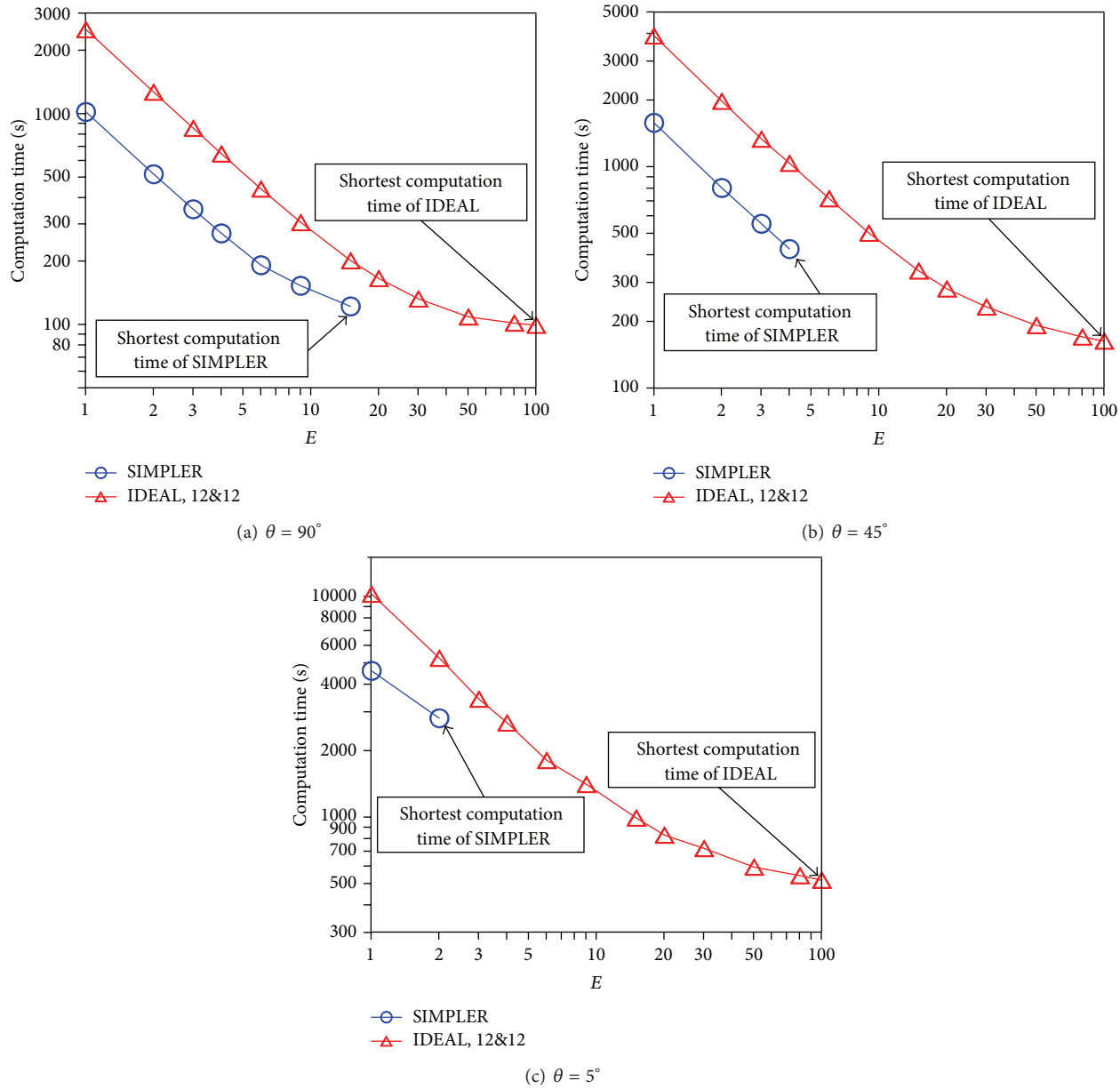

FIGURE 7: Comparison of computation time between IDEAL and SIMPLER for different inclination angles (Re = 500, grid number = 50 × 50 × 50).

Some correspondence between α and E is presented in Table 1. It can be seen that, with the time step multiple, we have a much wider range to show the performance of the algorithm in the high-value region of the underrelaxation factor.

4.2. Flow Configuration and Grid System of Lid-Driven Flow in 3D Inclined Cavity. In order to verify the feasibility of the IDEAL algorithm on highly skewed grid system, the lid-driven flow in the inclined cavity is calculated and analyzed. Its flow configuration is shown in Figure 2, where θ is the inclination angle and the length of each edge is equal to 1.

A transfinite interpolation method [30] is used to generate the body-fitted grid system for the inclined cavity. Figure 3 shows the generated grids for three different inclination angles. The grid skewness increases with the decrease of θ. As shown in this figure, the grids are skewed extremely high at $\theta = 5^\circ$.

The location of central line "CL" is shown in Figure 2. In Figure 4, the u velocity profiles along the central line "CL" are presented at $\theta = 5^\circ$ and Re = 500, where the Reynolds number is defined as

$$\mathrm{Re} = \frac{u_{\mathrm{lid}} H}{\nu}. \tag{10}$$

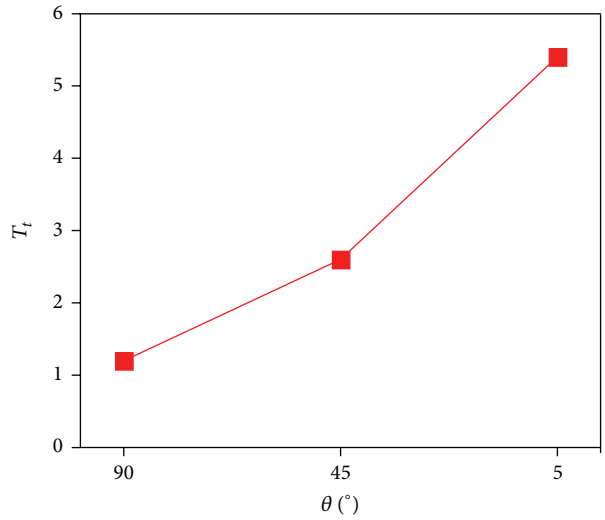

Figure 8: Times of the shortest time computation of SIMPLER over that of IDEAL for different inclination angles (Re = 500, grid number = 50 × 50 × 50).

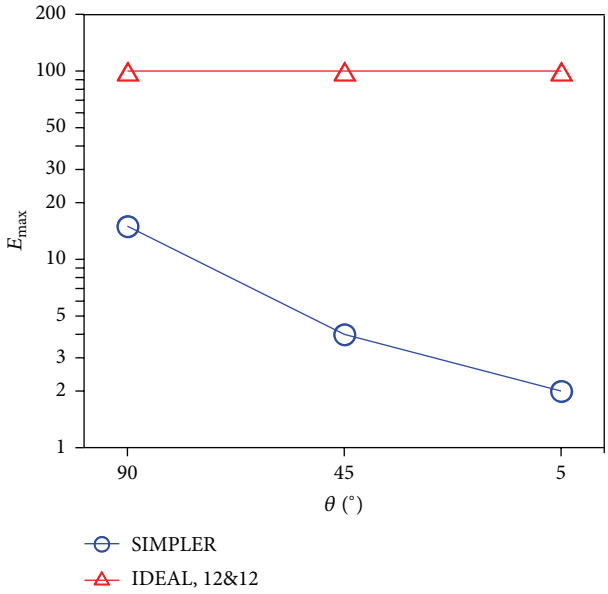

Figure 9: Comparison of the robustness between IDEAL and SIMPLER for different inclination angles (Re = 500, grid number = 50 × 50 × 50).

The results calculated by three different grid numbers are in excellent agreement with each other, proving that the IDEAL algorithm can obtain the grid-independent results. And the results calculated by the IDEAL algorithm agree very well with those calculated by the SIMPLER algorithm. These comparisons give some support to the reliability of the proposed IDEAL algorithm and the developed code.

4.3. Performance Analyses of IDEAL for Different Inclination Angles. Three different inclination angles ($\theta = 90^\circ, 45^\circ, 5^\circ$) are adopted to compare the solving performance between IDEAL and SIMPLER. Figure 5 shows the outer iteration numbers of IDEAL and SIMPLER for the three different inclination angles. And the minimum outer iteration numbers of IDEAL and SIMPLER are marked on this figure. Figure 6 shows the times of the minimum outer iteration number of SIMPLER over that of IDEAL, T_n, for the three different inclination angles. As shown in this figure, T_n increases with the decrease of the inclination angle. At $\theta = 5^\circ$, SIMPLER needs 3047 iterations to obtain the converged solution; however, IDEAL just needs 207 iterations. The value of T_n reaches up to 14.7.

Figure 7 shows the computation time of IDEAL and SIMPLER for the three different inclination angles. And the shortest computation times of IDEAL and SIMPLER are marked on this figure. Figure 8 shows the times of the shortest computation time of SIMPLER over that of IDEAL, T_t, for three different inclination angles. T_t is less than T_n. The reason is that the computation time of IDEAL used on each outer iteration level is longer than that of SIMPLER. When the grid is orthogonal, that is, $\theta = 90^\circ$, the shortest computation times of SIMPLER and IDEAL are, respectively, 122 s and 100 s; $T_t = 1.22$. The performance of IDEAL has a little improvement. When the grid is seriously skew, that is, $\theta = 5^\circ$, the shortest computation time of SIMPLER reaches up to 2817 s; however, IDEAL just needs 520 s; $T_t = 5.4$. The convergence rate of IDEAL is enhanced greatly.

Figure 9 compares the robustness between IDEAL and SIMPLER for three different inclination angles. Here, E_{max} denotes the maximum time step multiple that an algorithm can reach on the premise of obtaining the converged solution. The larger the value of E_{max} is, the more robust the algorithm is. For the SIMPLER algorithm, the robustness is weakened with the decrease of the inclination angle, due to the increase of the grid skewness. For the IDEAL algorithm, the inclination angle changes have no influence on the robustness. The value of E_{max} reaches up to 100. This means that it can converge almost at any time step multiple even in the case of $\theta = 5^\circ$.

Table 1: Some correspondence between α and E.

α	E
0.500	1
0.667	2
0.750	3
0.800	4
0.857	6
0.900	9
0.938	15
0.952	20
0.968	30
0.980	50
0.988	80
0.990	100

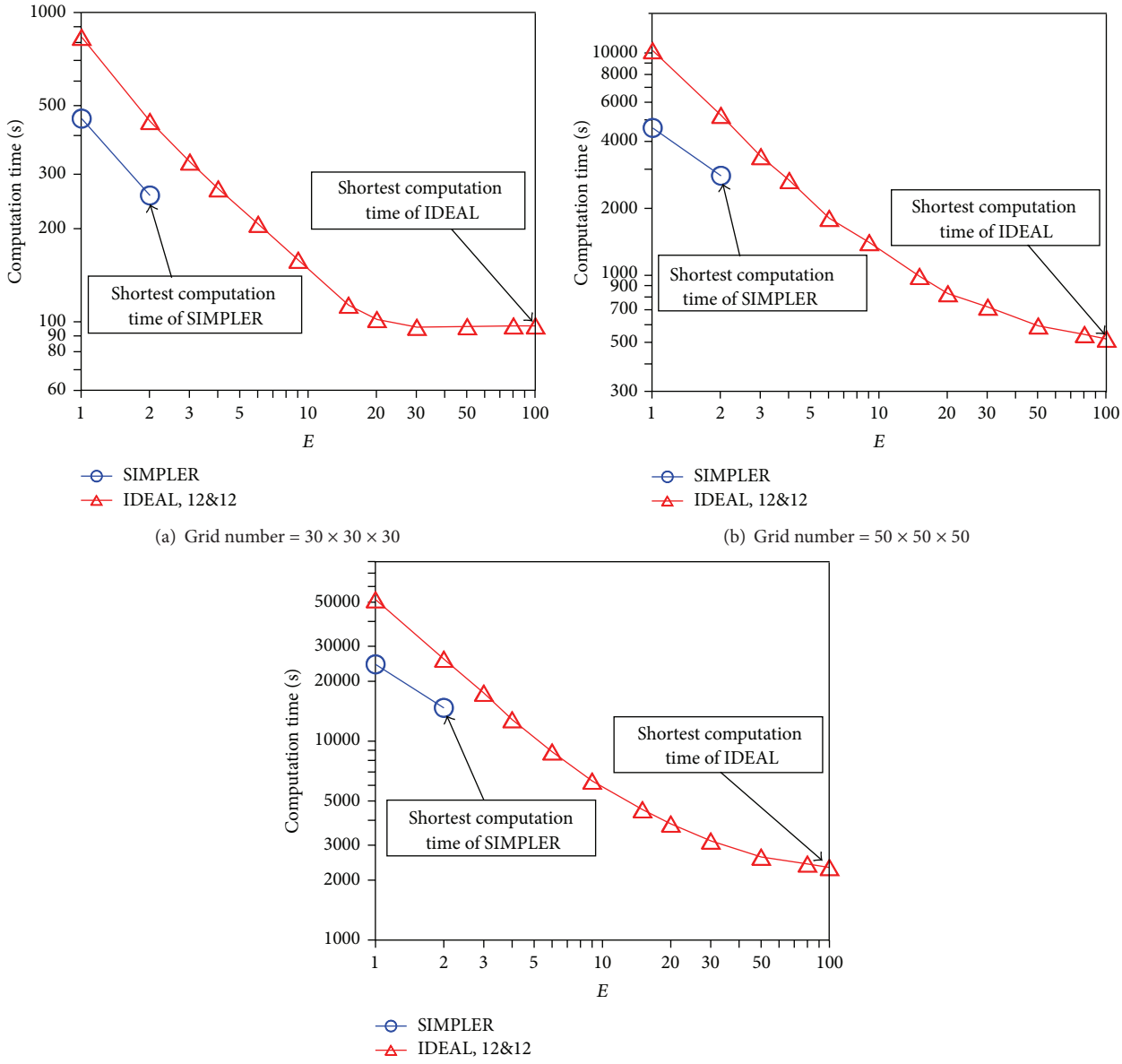

(a) Grid number = 30 × 30 × 30

(b) Grid number = 50 × 50 × 50

(c) Grid number = 70 × 70 × 70

FIGURE 10: Comparison of computation time between IDEAL and SIMPLER for different grid numbers (Re = 500, $\theta = 5^{\circ}$).

4.4. Performance Analyses of IDEAL for Different Grid Numbers. Three different grid systems of 30 × 30 × 30, 50 × 50 × 50, and 70 × 70 × 70 are considered at $\theta = 5^{\circ}$. All of the grids are skewed extremely highly. Figure 10 shows the computation time and marks the shortest computation time of IDEAL and SIMPLER for the three different grid numbers. The corresponding T_t is shown in Figure 11. T_t is greater than 1 and increases with the increase of the grid number. At grid number = 70 × 70 × 70, SIMPLER needs 14783 s to obtain the converged solution; however, IDEAL just needs 2330 s. The value of T_t reaches up to 6.3. Therefore, the IDEAL algorithm can significantly enhance the convergence rate compared with the SIMPLER algorithm, especially for the fine-grid flow case. Figure 12 compares the robustness between IDEAL and SIMPLER. The IDEAL algorithm can converge almost at any time step multiple ($E \leq E_{\max} = 100$) for the three different grid numbers. Its robustness is much better than that of the SIMPLER algorithm.

5. Conclusions

In this paper, the lid-driven flow in the inclined cavity has been adopted to compare the solving performance between IDEAL and SIMPLER. The following conclusions can be obtained.

(1) The IDEAL algorithm is more efficient than the SIMPLER algorithm for different inclination angles

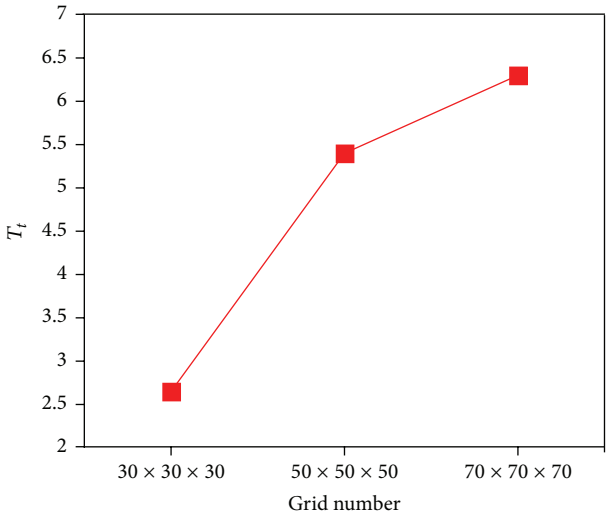

Figure 11: Times of the shortest time computation of SIMPLER over that of IDEAL for different grid numbers (Re = 500, $\theta = 5^\circ$).

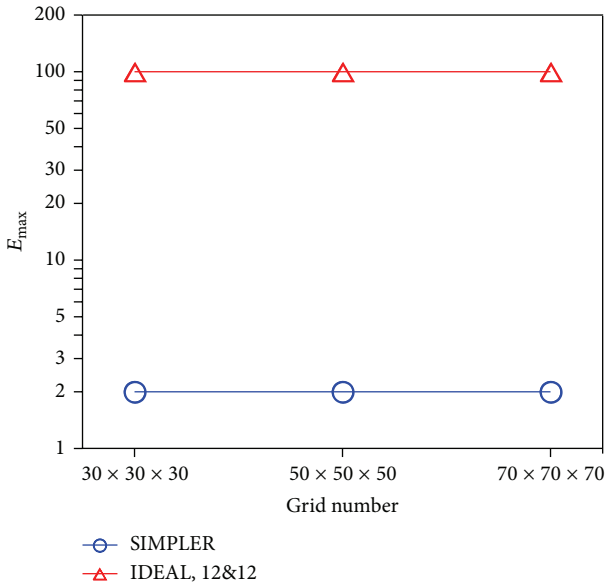

Figure 12: Comparison of the robustness between IDEAL and SIMPLER for different grid numbers (Re = 500, $\theta = 5^\circ$).

and different grid numbers, especially for the highly skewed and fine grid system. For example, at $\theta = 5^\circ$ and grid number = $70 \times 70 \times 70$, the convergence rate of the IDEAL algorithm is 6.3 times faster than that of the SIMPLER algorithm.

(2) The IDEAL algorithm is more robust than the SIMPLER algorithm for different inclination angles and different grid numbers. The IDEAL algorithm can converge almost at any time step multiple ($E \leq E_{max} = 100$) even in the case of $\theta = 5^\circ$ and grid number = $70 \times 70 \times 70$.

Due to the superiority of the IDEAL algorithm, it is expected that the proposed algorithm will be widely used in the future.

Nomenclature

a:	Coefficient in the discretized equation
b:	Constant term in the discretized equation
E:	Time step multiple
E_{max}:	Maximum time step multiple that an algorithm can reach
p:	Pressure, Pa
Re:	Reynolds number
S'_u, S'_v, S'_w:	Source term introduced by the grid nonorthogonality
T_n:	Times of the minimum outer iteration number of SIMPLER over that of IDEAL
T_t:	Times of the shortest computation time of SIMPLER over that of IDEAL
u,v, w:	Velocity components in x,y,and z directions, m·s^{-1}
U,V,W:	Contravariant velocity components in ξ, η, and ζ directions, m·s^{-1}
$\widetilde{U}$,$\widetilde{V}$,$\widetilde{W}$:	Pseudocontravariant velocities, m·s^{-1}
α:	Underrelaxation factor
η:	Dynamic viscosity, Pa·s
ν:	Kinematic viscosity, m^2·s^{-1}
θ:	Inclination angle, $^\circ$
ρ:	Density, kg·m^{-3}
ξ,η, ζ:	Nonorthogonal curvilinear coordinates.

Subscript

e,w,n,s,t,b:	Grid interface
nb:	Neighboring grid points
P,E,N,S,W,T,B:	Grid point
u,v,w:	Referring to u,v,and w momentum equations.

Superscript

p:	Referring to pressure equation
PTemp:	Temporary value in previous inner iteration step
Temp:	Temporary value in current inner iteration step
u,v, w:	Referring to u,v,and w momentum equations
0:	Previous iteration
$*$:	Intermediate value in iteration.

Conflict of Interests

The present authors declare that the paper does not have any conflict of interests including any financial, personal, or other relationships with other people or organizations.

Acknowledgments

This work was supported by the Program for New Century Excellent Talents in University (NCET-13-0792), the Natural Science Foundation of China of International Cooperation Project (Grant no. 51210011), the Young Scientists Fund of the National Natural Science Foundation of China (51106049), and the Program of the Coconstruction with Beijing Municipal Commission of Education of China.

References

[1] S. V. Patankar and D. B. Spalding, "A calculation procedure for heat, mass and momentum transfer in three-dimensional parabolic flows," *International Journal of Heat and Mass Transfer*, vol. 15, no. 10, pp. 1787–1806, 1972.

[2] S. V. Patankar, *Numerical Heat Transfer and Fluid Flow*, Hemisphere Series on Computational Methods in Mechanics and Thermal Science, Taylor & Francis, 1980.

[3] S. V. Patankar, "A calculation procedure for two-dimensional elliptic situations," *Numerical Heat Transfer*, vol. 4, no. 4, pp. 409–425, 1981.

[4] D. B. Spalding, "A general purpose computer program for multi-dimensional one- and two-phase flow," *Mathematics and Computers in Simulation*, vol. 23, no. 3, pp. 267–276, 1981.

[5] N. C. Markatos and K. A. Pericleous, "Laminar and turbulent natural convection in an enclosed cavity," *International Journal of Heat and Mass Transfer*, vol. 27, no. 5, pp. 755–772, 1984.

[6] J. P. van Doormaal and G. D. Raithby, "Enhancements of the SIMPLE method for predicting incompressible fluid flows," *Numerical Heat Transfer*, vol. 7, no. 2, pp. 147–163, 1984.

[7] R. I. Issa, "Solution of the implicitly discretised fluid flow equations by operator-splitting," *Journal of Computational Physics*, vol. 62, no. 1, pp. 40–65, 1985.

[8] R. I. Issa, A. D. Gosman, and A. P. Watkins, "The computation of compressible and incompressible recirculating flows by a non-iterative implicit scheme," *Journal of Computational Physics*, vol. 62, no. 1, pp. 66–82, 1986.

[9] J. P. van Doormaal and G. D. Raithby, "An evaluation of the segregated approach for predicting incompressible fluid flow," ASME Paper 85-HT-9, 1985.

[10] G. D. Raithby and G. E. Schneider, "Elliptic system: finite difference method," in *Handbook of Numerical Heat Transfer*, W. J. Minkowycz, E. M. Sparrow, R. H. Pletcher, and G. E. Schneider, Eds., John Wiley & Sons, New York, NY, USA, 1988.

[11] B. R. Latimer and A. Pollard, "Comparison of pressure-velocity coupling solution algorithms," *Numerical Heat Transfer*, vol. 8, no. 6, pp. 635–652, 1985.

[12] S. D. Connell and P. Stow, "The pressure correction method," *Computers and Fluids*, vol. 14, no. 1, pp. 1–10, 1986.

[13] X. Wen and D. B. Ingham, "New method for accelerating the rate of convergence of the SIMPLE-like algorithm," *International Journal for Numerical Methods in Fluids*, vol. 17, no. 5, pp. 385–400, 1993.

[14] T. Gjesdal and M. E. H. Lossius, "Comparison of pressure correction smoothers for multigrid solution of incompressible flow," *International Journal for Numerical Methods in Fluids*, vol. 25, no. 4, pp. 393–405, 1997.

[15] Y. Sheng, M. Shoukri, G. Sheng, and P. Wood, "A modification to the simple method for buoyancy-driven flows," *Numerical Heat Transfer B*, vol. 33, no. 1, pp. 65–78, 1998.

[16] T. Morii and K. Vierow, "The SOAR method for automatically optimizing SIMPLE relaxation factors," *Numerical Heat Transfer B*, vol. 38, no. 3, pp. 309–332, 2000.

[17] B. Yu, H. Ozoe, and W. Q. Tao, "A modified pressure-correction scheme for the SIMPLER method, MSIMPLER," *Numerical Heat Transfer B*, vol. 39, no. 5, pp. 435–449, 2001.

[18] X. L. Liu, W. Q. Tao, and Y. L. He, "A simple method for improving the SIMPLER algorithm for numerical simulations of incompressible fluid flow and heat transfer problems," *Engineering Computations*, vol. 22, no. 8, pp. 921–939, 2005.

[19] W. Q. Tao, Z. G. Qu, and Y. L. He, "A novel segregated algorithm for incompressible fluid flow and heat transfer problem—CLEAR (Coupled and Linked Equations Algorithm Revised). Part I—mathematical formulation and solution procedure," *Numerical Heat Transfer B*, vol. 45, no. 1, pp. 1–17, 2004.

[20] W. Q. Tao, Z. G. Qu, and Y. L. He, "A novel segregated algorithm for incompressible fluid flow and heat transfer problems—CLEAR (Coupled and Linked Equations Algorithm Revised). Part II—application examples," *Numerical Heat Transfer B*, vol. 45, no. 1, pp. 19–48, 2004.

[21] D. L. Sun, Z. G. Qu, Y. L. He, and W. Q. Tao, "An efficient segregated algorithm for incompressible fluid flow and heat transfer problems—IDEAL (Inner Doubly Iterative Efficient Algorithm for Linked Equations). Part I—mathematical formulation and solution procedure," *Numerical Heat Transfer B*, vol. 53, no. 1, pp. 1–17, 2008.

[22] D. L. Sun, Z. G. Qu, Y. L. He, and W. Q. Tao, "An efficient segregated algorithm for incompressible fluid flow and heat transfer problems—IDEAL (Inner Doubly Iterative Efficient Algorithm for Linked Equations). Part II—application examples," *Numerical Heat Transfer B*, vol. 53, no. 1, pp. 18–38, 2008.

[23] D. L. Sun, Z. G. Qu, Y. L. He, and W. Q. Tao, "Performance analysis of IDEAL algorithm for three-dimensional incompressible fluid flow and heat transfer problems," *International Journal for Numerical Methods in Fluids*, vol. 61, no. 10, pp. 1132–1160, 2009.

[24] D. L. Sun, Z. G. Qu, Y. He, and W. Tao, "Implementation of an efficient segregated algorithm-IDEAL on 3D collocated grid system," *Chinese Science Bulletin*, vol. 54, no. 6, pp. 929–942, 2009.

[25] D. L. Sun, Y. P. Yang, J. L. Xu, and W. Q. Tao, "Performance analysis of IDEAL algorithm combined with Bi-CGSTAB method," *Numerical Heat Transfer B*, vol. 56, no. 6, pp. 411–431, 2010.

[26] D. L. Son, W. Q. Tao, J. L. Xu, and Z. G. Qu, "Implementation of the IDEAL algorithm on nonorthogonal curvilinear coordinates for the solution of 3-d incompressible fluid flow and heat transfer problems," *Numerical Heat Transfer B*, vol. 59, no. 2, pp. 147–168, 2011.

[27] W. Q. Tao, *Numerical Heat Transfer*, Xi'an Jiaotong University Press, Xi'an, China, 2nd edition, 2001.

[28] Z. Y. Li and W. Q. Tao, "A new stability-guaranteed second-order difference scheme," *Numerical Heat Transfer B*, vol. 42, no. 4, pp. 349–365, 2002.

[29] S. Majumdar, "Roles of under-relaxation in momentum interpolation for calculation of flow with non-staggered grids," *Numerical Heat Transfer*, vol. 13, no. 1, pp. 125–132, 1988.

[30] W. Q. Tao, *Recent Advances in Computational Heat Transfer*, Science Press, Beijing, China, 2000.